

## Dynamic response of a linear two d.o.f system visco-elastically coupled with a rigid block

Angelo Di Egidio<sup>\*</sup>, Stefano Pagliaro<sup>a</sup>, Cristiano Fabrizio<sup>b</sup> and Andrea M. de Leo<sup>c</sup>

*DICEAA - University of L'Aquila, via G. Gronchi, 18-67100 L'Aquila, Italy*

*(Received February 27, 2019, Revised May 10, 2019, Accepted August 7, 2019)*

**Abstract.** The present work investigates the use of a rigid rocking block as a tool to reduce vibrations in a frame structure. The study is based on a simplified model composed by a *2-DOF* linear system, meant to represent a general *M-DOF* frame structure, coupled with a rocking rigid block through a linear visco-elastic device, which connects only the lower part of the *2-DOF* system. The possibility to restrain the block directly to the ground, by means of a second visco-elastic device, is investigated as well. The dynamic response of the model under an harmonic base excitation is then analysed in order to evaluate the effectiveness of the coupling in reducing the displacements and the drift of the *2-DOF* system. The non-linear equations of motion of the coupled assemblage *2-DOF-block* are obtained by a Lagrangian approach and then numerically integrated considering some reference mechanical and geometrical quantities as variable parameters. It follows an extensive parametric analysis, whose results are summarized through behaviour maps, which portray the ratio between the maximum displacements and drifts of the system, with and without the coupling with the rigid block, for several combinations of system's parameters. When the ratio of the displacements is less than unity, the coupling is considered effective. Results show that the presence of the rocking rigid block improves the dynamics of the system in large ranges of the characterizing parameters.

**Keywords:** visco-elastic coupling; rocking rigid block; harmonic excitation; gain coefficients and maps

### 1. Introduction

Frame structures can be coupled with other mechanical systems (i.e., mechanical devices or other structures) to improve their behaviour under external loads. Some examples of such mechanical devices are oscillating masses working as tuned mass dampers, dynamic mass absorbers and elasto-plastic dampers. Among others possibilities to improve the dynamic behaviour of a frame structure, the conjunction with a rocking rigid block can be envisaged, on the basis of the intrinsic energy dissipating characteristics of the rocking motion. To the comprehension of the behaviour of such a

---

<sup>\*</sup>Corresponding author, Associate Professor, Angelo Di Egidio, E-mail: [angelo.diegidio@univaq.it](mailto:angelo.diegidio@univaq.it)

<sup>a</sup>Ph.D. student, E-mail: [stefano.pagliaro@graduate.univaq.it](mailto:stefano.pagliaro@graduate.univaq.it)

<sup>b</sup>Ph.D., E-mail: [cristiano.fabrizio@graduate.univaq.it](mailto:cristiano.fabrizio@graduate.univaq.it)

<sup>c</sup>Ph.D., E-mail: [ing.andrea.deleo@gmail.com](mailto:ing.andrea.deleo@gmail.com)

mechanical system several papers have been dedicated, starting from the pioneering work of Housner (Housner (1963)). Both the seismic excitation (Yim *et al.* (1980), Pompei *et al.* (1998), Taniguchi (2002), Psycharis *et al.* (2013) and other kinds of ground excitation, such as harmonic or impulsive one-sine excitation (Spanos and Koh (1984), Zhang and Makris (2001), Kounadis (2013), Vassiliou *et al.* (2014)) and random excitation (Spanos and Koh (1986)) were considered.

In several papers a general formulations for the rocking and slide-rocking motions of free-standing symmetric rigid blocks (Andreaus (1990), Shenton and Jones (1991), VoyagakiIoannis *et al.* (2013)) was proposed. In Shenton (1996), Tung (2007) the analysis of the different phases of motions and the definition of criteria for the transition between them were performed. In some papers either non-symmetric rigid blocks (Contento and Di Egidio (2009)), or three-dimensional blocks (Zulli *et al.* (2012), Di Egidio *et al.* (2014b, 2015)) were considered. Other papers studied the dynamics of rigid blocks in a general way (DeJong and Dimitrakopoulos (2014)). In Spanos *et al.* (2017) an interesting experimental investigation of a block on a non-linear deformable foundation was performed.

Recently many papers have studied the coupling of the block with different passive or active devices in order to protect them from the overturning. For example, the effectiveness of base anchorages was studied in Makris and Zhang (2001), Dimitrakopoulos and DeJong (2012) in order to protect rigid blocks from overturning, whereas Di Egidio and Contento (2009, 2010), Contento and Di Egidio (2014), Caliò and Marletta (2003), Vassiliou and Makris (2012) highlighted the efficiency of the base isolated system. Other types of passive control methods for the protection of rigid blocks were considered, for example, in Corbi (2006) the authors proposed a sloshing water damper. A mass-damper dynamic absorber in the shape of a pendulum was used by different authors (Collini *et al.* (2016), Brzeski *et al.* (2016), de Leo *et al.* (2016)), who demonstrated the general effectiveness of this kind of protection device. Instead, in Simoneschi *et al.* (2017a, b), Di Egidio *et al.* (2018) a mass-damper modelled as a single degree of freedom and running on the top of the block was considered as safety device.

Also active or semi-active devices were used to improve the dynamic and seismic performances of blocks. For example Ceravolo *et al.* (2016) and Ceravolo *et al.* (2017) studied the use of semi-active anchorages using feedback-feedforward or a feedback strategies to increase the acceleration required to topple a reference block. Recently Di Egidio *et al.* (2014a), Simoneschi *et al.* (2018) used an active control technique based on the Pole Placement approach to increase the amplitude of the base excitation able to topple a rigid block.

An interesting topic that is increasingly present in the Scientific Literature regards the dynamic improvement of structures by coupling them with other structures of the same type or of different type. In this field some papers (Ormeño *et al.* (2012), Khatiwada *et al.* (2013), Huang *et al.* (2013), Muratović and Ademović (2015)) represent an example. Specifically, in Huang *et al.* (2013), Muratović and Ademović (2015) particular attention was devoted to the coupling between a frame structure and a rocking wall. However, the use of rocking rigid block as a protecting device of other kinds of structure represents a particular issue, not frequently dealt with, to which the present work intends to provide some contributions. Differently from some recent works Aghagholizadeh and Makris (2018), Makris and Aghagholizadeh (2017) in which the authors investigated a rigid coupling between a frame and a rocking wall under seismic excitations, this paper analyses a linear visco-elastic coupling of a frame structure and a rigid block aimed at improving the dynamic behaviour of the frame (i.e. reducing horizontal displacements and drifts). A two-degree of freedom linear system is used as model for a

multi-story frame structure. A first visco-elastic device connects the block to the lower part of the frame structure. A second visco-elastic device connects the block directly to the ground. Such devices are respectively called *coupling* (CD) and *external* device (ED) in the following sections. The non-linear equations of motion of the coupled-system are obtained by a Lagrangian approach and successively numerically integrated to analyze the behaviour of the coupled system. Simulations are performed using an harmonic base excitation. An extensive parametric analysis, based on the variation of some mechanical and geometrical parameters, is performed, and the results are summarized by means of *gain maps*. The maps show the ratio between the maximum displacements or drifts of the coupled and uncoupled frame in different planes of the system's parameters.

## 2. Reference mechanical assemblage

The analyses hereby presented are based on the reference mechanical system portrayed in Figure 1, in which a rocking rigid block is connected, through a non rigid link, to the lower level of a frame structure with the aim the reduce its side displacements and drifts deriving from a base horizontal motion. Such an assemblage presents some consistent differences with respect to recent papers (Aghagholizadeh and Makris (2018) and Makris and Aghagholizadeh (2017)) which considered instead a full height rigid connection between a frame and a rocking wall (i.e., rigid connection at each level).

The specific proposed configuration, with the block shorter than the frame and located underneath the frame's foundation level, derives from some considerations that follows. On the one hand a shorter block may result in a more feasible solution, as its functional and aesthetic impact can be limited together with the concern for the outside safety in case of overturn. Moreover a shorter block avoids any possible interaction with the upper levels of the frame. On the other hand, in order to have enough mass for the block and sufficient stroke length for its head (where the connection is foreseen) the block should be lowered within a trench or a pit.

## 3. Analytical model of the coupled system

With reference to Fig. 2(a), the analytical model of the coupled system is composed by an homogeneous parallelepiped rigid block, with a mass  $M = \rho \times 2b \times 2h_b \times s$ , where  $\rho = 2500 \text{ kg/m}^3$  and  $s$  is the dimension orthogonal to the plane of the figure.

The block is connected with a reduced order *2-DOF* model, considered representative of the frame structure. The two 2 degrees of freedom associated to the frame allow, on the one hand, the representation of the partial conjunction, on the other hand, the detection of the drifts. The mechanical characteristics of the *2-DOF* model (stiffness  $k_j$ , damping constant  $c_j$  and mass  $m_j$ ,  $j = 1, 2$ ), in such a way it is dynamically equivalent to the multi-degree of freedom frame, are evaluated following the equivalence procedure exposed in Fabrizio *et al.* (2017b, 2019, 2017a). In principle, since the recalled procedure associates the masses  $m_1$  and  $m_2$  to the physical masses of the two portion of the frame (connected lower sub-structure and unconnected upper sub-structure) the dimensions  $h_1$ ,  $h_2$  (Fig. 2a) can be measured directly from the mechanical assemblage of Fig. 1.

Two linear visco-elastic devices, represented by a couple of spring and dash-pot (stiffness  $k_i$ , damping constant  $c_i$ ,  $i = C, E$ ) are considered within the model. The first one (*CD Coupling device*)

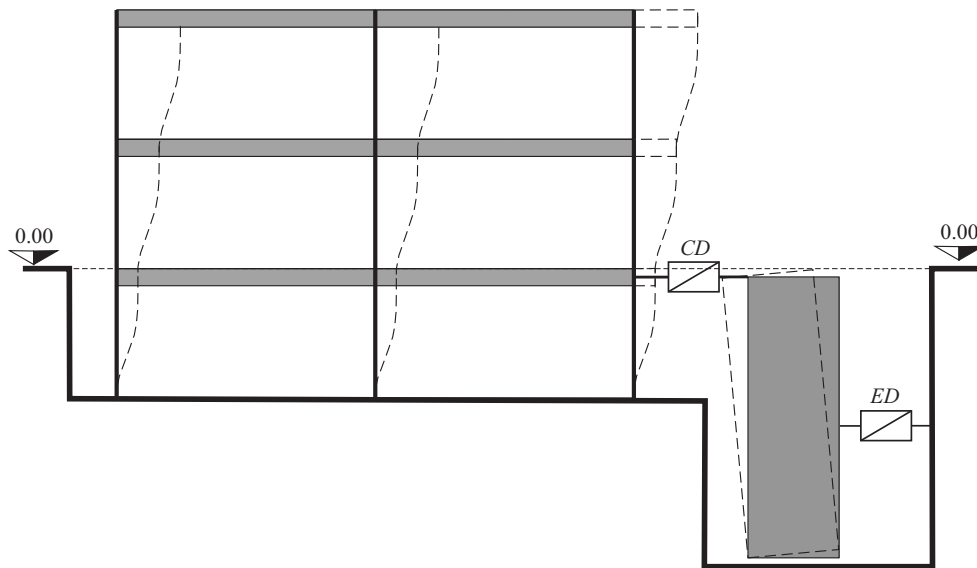


Fig. 1 Coupling between a frame structure and the rocking wall (*CD*: Connecting Device - *ED*: External Device)

connects the lower part of the system and the top of the block; the second one (*ED* External device), that might be absent, links the block to the ground (Fig. 2a).

### 3.1 Equations of motion for rocking of the block around the left corner

It is assumed that the block cannot slide, therefore only rocking motions can occur. Consequently, three Lagrangian parameters fully describe the motion. Such parameters are the displacements (relative to the ground) of the two d.o.f. system  $u_1$  and  $u_2$ , and the rotation of the block  $\vartheta$ . Figure 2b shows the positive directions of the three Lagrangian parameters. Two sets of three equations of motion, which describe the motion of the system when the block rocks around either the left corner  $A$  or the right corner  $B$ , have to be obtained. For the sake of brevity, in this section, only the relationships needed to describe the motion of the system when the block is rocking around the left corner  $A$  are reported. The equations describing the rocking of the block around the right corner are reported in Appendix A.

In order to write the equations of motion of the mechanical system via a Lagrangian approach, the positions of the mass centres of the bodies are evaluated. For this purpose, an inertial reference frame with origin in  $O$ , initially coincident with the left base corner  $A$  of the block, is considered (Fig. 2a). The positions of the mass centres  $G_1$  and  $G_2$  of the two d.o.f. structure are:

$$\mathbf{x}_{G1}(t) = \begin{Bmatrix} x_g(t) - d - d_G + u_1(t) \\ d_h + h_1 \\ 0 \end{Bmatrix}; \quad \mathbf{x}_{G2}(t) = \begin{Bmatrix} x_g(t) - d - d_G + u_2(t) \\ d_h + h_2 \\ 0 \end{Bmatrix} \quad (1)$$

The position of the mass centre  $C$  of the block during a rocking around the left corner  $A$  reads:

$$\mathbf{x}_C(t) = \begin{Bmatrix} x_g(t) \\ 0 \\ 0 \end{Bmatrix} + \begin{bmatrix} \text{Cos}\vartheta(t) & -\text{Sin}\vartheta(t) & 0 \\ \text{Sin}\vartheta(t) & \text{Cos}\vartheta(t) & 0 \\ 0 & 0 & 1 \end{bmatrix} \begin{Bmatrix} b \\ h_b \\ 0 \end{Bmatrix} \quad (2)$$

where the matrix in Eq. (2) is the rotation tensor of the block. The kinetic energy of the mechanical system during a rocking motion of the block around the left corner *A* reads:

$$T = \frac{1}{2} \left[ \sum_{i=1}^2 m_i (\dot{\mathbf{x}}_{Gi}(t) \cdot \dot{\mathbf{x}}_{Gi}(t)) + J_C (\dot{\theta}(t) \cdot \dot{\theta}(t)) + M (\dot{\mathbf{x}}_C(t) \cdot \dot{\mathbf{x}}_C(t)) \right] \quad (3)$$

where  $\dot{\theta}(t) = \{0, 0, \dot{\vartheta}(t)\}^T$  and  $J_C$  is the polar inertia of the block with respect to its centre of mass. In order to evaluate the potential energy for a rocking motion around the corner *A*, the distance vectors between the couples of points *W, K* and *Z, Y* have to be evaluated. They are required to compute the potential energy associate to the elastic devices that have stiffness  $k_C$  and  $k_E$ . The positions of these points read:

$$\begin{aligned} \mathbf{x}_W(t) &= \begin{Bmatrix} -d + x_g(t) + u_1(t) \\ d_h + h_1 \\ 0 \end{Bmatrix}; & \mathbf{x}_Y(t) &= \begin{Bmatrix} x_g(t) + 2b + a \\ d_e \\ 0 \end{Bmatrix}; \\ \mathbf{x}_K(t) &= \begin{Bmatrix} x_g(t) \\ 0 \\ 0 \end{Bmatrix} + \begin{bmatrix} \text{Cos}\vartheta(t) & -\text{Sin}\vartheta(t) & 0 \\ \text{Sin}\vartheta(t) & \text{Cos}\vartheta(t) & 0 \\ 0 & 0 & 1 \end{bmatrix} \begin{Bmatrix} 0 \\ d_h + h_1 \\ 0 \end{Bmatrix}; & (4) \\ \mathbf{x}_Z(t) &= \begin{Bmatrix} x_g(t) \\ 0 \\ 0 \end{Bmatrix} + \begin{bmatrix} \text{Cos}\vartheta(t) & -\text{Sin}\vartheta(t) & 0 \\ \text{Sin}\vartheta(t) & \text{Cos}\vartheta(t) & 0 \\ 0 & 0 & 1 \end{bmatrix} \begin{Bmatrix} 2b \\ d_e \\ 0 \end{Bmatrix} \end{aligned}$$

Then, the distance vectors between the previous couples of points, read:

$$\begin{aligned} \mathbf{x}_{WK}(t) = \mathbf{x}_K(t) - \mathbf{x}_W(t) &= \begin{Bmatrix} d - \text{Sin}\vartheta(t)(d_h + h_1) - u_1(t) \\ -d_h - h_1 + \text{Cos}\vartheta(t)(d_h + h_1) \\ 0 \end{Bmatrix} \\ \mathbf{x}_{ZY}(t) = \mathbf{x}_Y(t) - \mathbf{x}_Z(t) &= \begin{Bmatrix} a + 2b - 2b\text{Cos}\vartheta(t) + d_e\text{Sin}\vartheta(t) \\ d_e - d_e\text{Cos}\vartheta(t) - 2b\text{Sin}\vartheta(t) \\ 0 \end{Bmatrix} \end{aligned} \quad (5)$$

The potential energy of the system then reads;

$$V = [Mg (\mathbf{x}_C(t) - \bar{\mathbf{x}}_C) \cdot \mathbf{j}] + \frac{1}{2} [k_1 u_1(t)^2 + k_2 (u_2(t) - u_1(t))^2] + \frac{1}{2} \left[ k_C \left( \sqrt{\mathbf{x}_{WK}(t) \cdot \mathbf{x}_{WK}(t)} - d \right)^2 + k_E \left( \sqrt{\mathbf{x}_{ZY}(t) \cdot \mathbf{x}_{ZY}(t)} - a \right)^2 \right] \quad (6)$$

where *g* is the gravity acceleration,  $\mathbf{j} = \{0, 1, 0\}^T$  is the unity vector of the *y*-axis,  $\bar{\mathbf{x}}_C = \{b, h_b, 0\}^T$  is the positions of the mass centre corresponding to the minimum potential energy of the system. Since it is constant, it consequently plays no role in the derivation of the equations of motion.

Due to the presence of dash-pots with damping coefficients  $c_1$ ,  $c_2$ ,  $c_C$  and  $c_E$  (Fig. 2(a)), the virtual work  $\delta W$  of the non-conservative viscous forces has to be considered to obtain the Lagrangian equations of motion; it reads:

$$\delta W = - [c_1 \dot{u}_1(t) \delta u_1(t) + c_2 (\dot{u}_2(t) - \dot{u}_1(t)) (\delta u_2(t) - \delta u_1(t))] - [c_C (\mathbf{x}_{WK}(t) \cdot \delta \mathbf{x}_{WK}(t)) + c_E (\mathbf{x}_{ZY}(t) \cdot \delta \mathbf{x}_{ZY}(t))] \quad (7)$$

Finally, the equation of motion can be obtained by:

$$\left[ \frac{d}{dt} \left( \frac{\partial L}{\partial \dot{q}_i} \right) - \frac{\partial L}{\partial q_i} \right] \delta q_i = \delta W(\delta q_i), \quad \forall \delta q_i \neq 0; (i = 1, 2, 3) \quad (8)$$

where  $L = T - V$  is the Lagrangian function,  $(q_1, q_2, q_3) = (u_1, u_2, \vartheta)$  and  $(\delta q_1, \delta q_2, \delta q_3) = (\delta u_1, \delta u_2, \delta \vartheta)$ . The equations of motion then read:

$$\begin{aligned} & -k_C (d - (d_h + h_1) \sin \theta - u_1) \times Q_1 + \\ & c_C ((d_h + h_1) \theta' \cos \theta + \dot{u}_1) + (c_1 + c_2) \dot{u}_1 - \\ & c_2 \dot{u}_2 + (k_1 + k_2) u_1 - k_2 u_2 + m_1 (\ddot{x}_g + \ddot{u}_1) = 0 \\ & \text{-----} \\ & c_2 (\dot{u}_2 - \dot{u}_1) + k_2 (u_2 - u_1) + m_2 (\ddot{x}_g + \ddot{u}_2) = 0 \\ & \text{-----} \\ & k_E (\sin \theta (2b(a + 2b) + d_e^2) + ad_e \cos) \times Q_2 + \\ & 4b^2 c_E \dot{\theta} + \cos \theta (bgM + c_C (d_h + h_1) \dot{u}_1 - h_b M \ddot{x}_g) - M \sin \theta (b \ddot{x}_g + gh_b) + \\ & k_C (d_h + h_1) ((u_1 - d) \cos \theta + (d_h + h_1) \sin \theta) \times Q_1 + \\ & c_E d_e^2 \dot{\theta} + c_C d_h^2 \dot{\theta} + 2c_C d_h h_1 \dot{\theta} + c_C h_1^2 \dot{\theta} + J_A \ddot{\theta} = 0 \end{aligned} \quad (9)$$

where:

$$\begin{aligned} Q_1 &= \frac{(\sqrt{d^2 - 2(d-u_1)(d_h+h_1) \sin \theta - 2du_1 + 2d_h^2 - 2(d_h+h_1)^2 \cos \theta + 4d_h h_1 + 2h_1^2 + u_1^2 - d})}{\sqrt{d^2 - 2(d-u_1)(d_h+h_1) \sin \theta - 2du_1 + 2d_h^2 - 2(d_h+h_1)^2 \cos \theta + 4d_h h_1 + 2h_1^2 + u_1^2}} \\ Q_2 &= \frac{(\sqrt{a^2 - 2 \cos \theta (2b(a+2b) + d_e^2) + 4ab + 2ad_e \sin \theta + 8b^2 + 2d_e^2 - a})}{\sqrt{a^2 - 2 \cos \theta (2b(a+2b) + d_e^2) + 4ab + 2ad_e \sin \theta + 8b^2 + 2d_e^2}} \end{aligned} \quad (10)$$

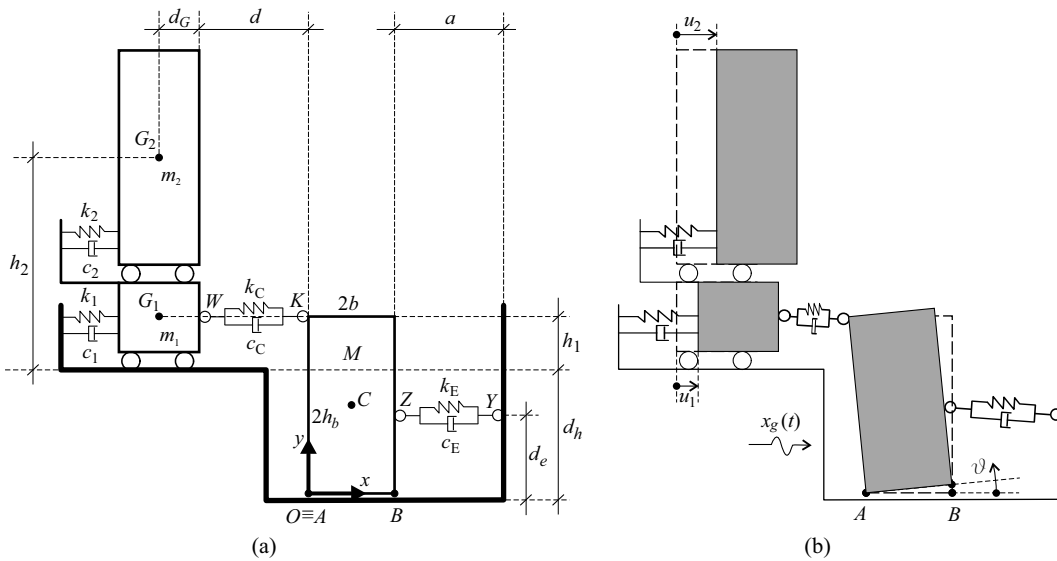


Fig. 2 Mechanical system: (a) Geometrical characterization of the system and (b) Lagrangian parameters (positive directions)

### 3.2 Uplift and impact conditions

The uplift of the block around point  $A$  takes place when the resisting moment  $M_R = Mgb$ , due to the weight of the block gets smaller than the overturning moment  $M_O = -M\ddot{x}_g(t)h_b + [k_C u_1(t) + c_C \dot{u}_1(t)](d_h + h_1)$  due to the inertial forces and to the visco-elastic ones of the internal coupling device. It should be noted that as long as the block doesn't tilt, there's no stroke for the external device, thus its contribution to  $M_O$  is null (Fig. 2(b)). All these moments are evaluated with respect to the base point  $A$  (Fig. 2(a)). By vanishing the sum of the two previous moments, it is possible to obtain the external acceleration  $\ddot{x}_g$  able to uplift the block. Such an acceleration reads:

$$\ddot{x}_g = \frac{g}{\lambda} + \frac{[k_C u_1(t) + c_C \dot{u}_1(t)](d_h + h_1)}{Mh_b} \tag{11}$$

where  $\lambda = h_b/b$  is the slenderness of the block. In absence of the coupling with the device, the uplift condition is the same of a stand-alone block.

During the rocking motion, when the rotation  $\vartheta(t)$  approaches zero, an impact between the block and the ground occurs. Post-impact conditions of the rocking motion can be found assuming that the impact happens instantly, the body position remains unchanged, and the angular momentum is maintained. This condition can be expressed as  $(J_O - 2bS_y)\dot{\vartheta}^- = J_O\dot{\vartheta}^+$ , where  $J_O$  is the polar inertia of the block with respect to one of the two base corners  $A$  or  $B$ ;  $S_y = Mb$  is the static moment of the block with respect to a vertical axis passing through one of the two base corners (after some algebra the conservation of the angular momentum becomes as in Housner (1963)). Since the block is symmetric, it follows  $J_O = J_A = J_B$ , then the impact conditions referring to a block that after an impact re-uplifts around the corner  $A$  or  $B$  are equal. Superscript  $(\cdot)^-$  and superscript  $(\cdot)^+$  denote pre- and post-impact quantities, respectively. From the conservation of the angular momentum, the maximum value of the post-impact angular velocity  $\dot{\vartheta}^+$  can be obtained as a function of the pre-impact

angular velocity  $\dot{\vartheta}^-$ . The post-impact angular velocity that is considered in the numerical simulations is equal to  $\dot{\vartheta}^+ = \eta [(J_O - 2b S_y)/J_O] \dot{\vartheta}^-$  where  $\eta$  is a coefficient less than unity, introduced to include a further loss of mechanical energy. In the analyses, the value of  $\eta$  is fixed ( $\eta = 0.9$ ) (Aghagholizadeh and Makris (2018), Makris and Aghagholizadeh (2017)).

### 3.3 Linearized equations of motion

As a support for the interpretation of the results, a comparison will be performed with the outcomes of a linearized formulation, based on the hypotheses of small rotations  $\vartheta$  and small damping for all the dash-pots. The linearised equations of motion of the coupled, undamped, homogeneous system are obtained by expanding in McLaurin series up to the first order the non-linear equations of motion Eq. (8), with respect to the Lagrangian parameters  $u_1, u_2$  and  $\vartheta$ . The equations below refers to the rocking of the block around the left corner  $A$  and read:

$$\mathbf{M}\ddot{\mathbf{X}} + \mathbf{K}\mathbf{X} = \mathbf{0} \quad (12)$$

where

$$\mathbf{M} = \begin{bmatrix} m_1 & 0 & 0 \\ 0 & m_2 & 0 \\ 0 & 0 & J_A \end{bmatrix}; \quad \mathbf{X} = \begin{Bmatrix} u_1 \\ u_2 \\ \vartheta \end{Bmatrix} \quad (13)$$

$$\mathbf{K} = \begin{bmatrix} k_1 + k_2 + k_C & -k_2 & (d_h + h_1)k_C \\ -k_2 & k_2 & 0 \\ (d_h + h_1)k_C & 0 & -h_b Mg + d_e^2 k_E + (d_h + h_1)^2 k_C \end{bmatrix}$$

The frequencies and the modes of the coupled system are obtained by solving the following eigenproblem:

$$(\mathbf{K} - \omega^2 \mathbf{M})\mathbf{U} = \mathbf{0} \quad (14)$$

where  $\omega$  is the eigenvalue (linearised circular frequency) of the system and  $\mathbf{U}$  is the eigenvector (vibration mode). It can be demonstrated that for dimensions of the block of practical interest, the positive definiteness of the stiffness matrix  $\mathbf{K}$  is always guaranteed. The linearised system admits then three frequencies (real and positive) and three modes.

The linearised equations of motion referring to the block that rocks around the right corner  $B$  are exactly equal to Eq. (12) and Eq. (13). Formally, only the term  $J_A$  in the mass matrix  $\mathbf{M}$  (Eq. (13)) change in  $J_B$ . However, due to the assumed symmetry of the block, it follows that  $J_A = J_B$  (*i.e.* the polar inertia of the block around the two base corners are equal).

## 4. Parametric analysis

An extensive parametric analysis is performed to investigate the behaviour of the coupled system by numerically integrating the equations of motion. Special care is devoted to the detection of the impacts of the block. In the performed analyses, the block never exceeds the critical angle  $\alpha_C = \arctan(b/h_b)$  (*i.e.* the centre  $C$  of the block is inside the vertical projection of the base, thus no overturning occurs).

In the parametric analyses, the 2-DOF model refers to two building frames with different characteristics. The first one is small building of three equal stories, each one of surface of  $100,00m^2$ . The

Table 1 Characteristics of the two buildings

Stories	Connection Level	Story surface	Story mass $m_s$	Story height
3	1	100 m <sup>2</sup>	120.6x10 <sup>3</sup> kg	3 m
5	2	250 m <sup>2</sup>	301.5x10 <sup>3</sup> kg	3 m

Table 2 Characteristics of the 2 d.o.f. representing the buildings ( $\omega_{unc}$  is the circular frequency of the first mode of the uncoupled system.)

Stories	$k_1$ (N/m)	$k_2$ (N/m)	$m_1$ (kg)	$m_2$ (kg)	$\omega_{unc}$ (rad/s <sup>-1</sup> )	$\xi$
3	2.194415x10 <sup>8</sup>	9.404636x10 <sup>7</sup>	120.6x10 <sup>3</sup>	241.2x10 <sup>3</sup>	16.02	0.05
5	7.641287x10 <sup>8</sup>	1.819354x10 <sup>8</sup>	241.2x10 <sup>3</sup>	361.8x10 <sup>3</sup>	10.65	0.05

second building has five equal stories of surface of 250,00m<sup>2</sup>. Both the buildings have the inter-story height of 3.0m. The displacement  $u_1$  refers to the story where there is the connection with the block (sub-structure). The displacement  $u_2$  represents the displacement of the highest story of the structure (super-structure). The values of the stiffness,  $k_1$  and  $k_2$ , are evaluated by using the procedure in Fabrizio *et al.* (2017b, 2019, 2017a). In Table 1 are shown the main characteristics of the two considered buildings, whereas in Table 2 are reported the main characteristics of the 2-DOF systems, representing the two buildings.

The harmonic excitation used in the analyses is  $\ddot{x}_g(t) = A_s \sin(\Omega t)$ ,  $0 \leq t \leq t_{max}$ , where  $\Omega = 2\pi/T_s$  is the circular frequency  $T_s$  is the period of the harmonic cycle,  $A_s$  is its amplitude and  $t_{max}$  is the maximum time used in the numerical integrations ( $t_{max} = 25 T_s$ ). Since the mechanical system is non-linear, its behaviour depends on the amplitude  $A_s$  of the excitation. However, some preliminary tests showed that, for values of the block rotation sufficiently smaller than the critical angle  $\alpha_C$ , the dependence of the motion on the amplitude itself is minimal. Hence, in the numerical simulations, the amplitude is fixed at  $A_s = 5.0 m/s^2$ .

The following parametrization is used to improve the understanding of the results:

$$k_C = \beta k_1, k_E = \gamma k_1 \tag{15}$$

#### 4.1 Numerical integration

The numerical integration of the equations of rocking motion Eq. (9) and Eq. (A.1), taking into account the uplift conditions Eq. (11) and Eq. (A.3) and the impact conditions, is performed by an original code developed by the same Authors of this paper.

The procedure is programmed to detect, from the first step of integration, the achievement of the uplift condition expressed by Eqs. (11) or (A.3). As long as these conditions are not verified, only the equations of motion for the sole 2-DOF are integrated. Then, once the block starts to uplift according to Eqs. (11) or (A.3), the algorithm starts with the integration of equation Eq. (9) for the rocking around the left corner  $A$  or Eq. (A.3) for the rocking around the right corner  $B$ , assuming as initial conditions for the 2-DOF, the values of  $u_1, u_2$  and  $\dot{u}_1, \dot{u}_2$  obtained at the end of the previous integration step.

After each integration step  $i$ , a check is made on the rocking angle  $\vartheta$ . If  $\vartheta_{t_{i-1}} * \vartheta_{t_i} < 0$ , it means that an impact has occurred and the algorithm switches from a set of rocking equations to the other one

by reducing the post-impact angular velocity  $\dot{\vartheta}^+ = \eta [(J_O - 2b S_y)/J_O]\dot{\vartheta}^-$ , as already explained in Section 3.2 - *Uplift and impact conditions*. During the integration two checks are performed to stop the integration procedure. One of these, stops the numerical integration if the final time  $t_{max}$  is reached; the other checks if an overturning of the the block occurred.

The code is developed in *Mathematica*<sup>®</sup> environment and makes use of the built-in integration function *NDSolve* (<http://www.wolfram.com/mathematica/>) to integrate numerically the equations of motion. The function *NDSolve* automatically transforms the equations Eq. (9) and Eq. (A.1) in a normal form system of first-order ordinary differential equations. The classical four-order Runge-Kutta method is selected as internal integration method. The time step used in the numerical integration is  $\Delta_t = 0.001s$ , that assures a good accuracy in the evaluation of the times at which an impact occurs.

#### 4.2 Gain coefficients

The displacement  $u_1$  and the overall drift  $u_2 - u_1$  are used as indicators to evaluate the dynamic performance of the system. The smaller  $u_1$  and  $u_2 - u_1$  are, the greater is the effectiveness of the coupling with the block. As done in Fabrizio *et al.* (2017b), two gain parameters are then introduced:

$$\alpha_1 = \frac{\max |u_1(t)|}{\max |\tilde{u}_1(t)|}, \quad \alpha_2 = \frac{\max |u_2(t) - u_1(t)|}{\max |\tilde{u}_2(t) - \tilde{u}_1(t)|} \quad (16)$$

where the displacements  $\tilde{u}_1$  and  $\tilde{u}_2$  refer to the uncoupled bare frame structure. If the parameters of Eq. (16) are less than unity, the coupling between the frame structure and the rocking block is beneficial for the frame structure. An extensive parametric analysis is performed with the aim to build gain maps that represent the values of  $\alpha_1$  and  $\alpha_2$  in specific parameters planes.

#### 4.3 The role of the coupling visco-elastic device

The first parametric analysis investigates the influence of the coupling visco-elastic device (i.e., the internal device *CD*) on the motion of the structure. In this analysis, the external device *ED* connecting the block with the ground is neglected ( $k_E = c_E = 0$ , see Fig.2). The parameters that are varied in the analysis are the base of the block,  $2b$ , and the stiffness ratio  $\beta$  of the coupling device (Eq. (15)). The range of variation of the block base  $2b$  goes from  $2b = 0.2m$  to  $2b = 2.0m$ . These values correspond to blocks with mass  $M$  that ranges from about 4% to 40% of the total mass of the *2-DOF* system. The stiffness of the coupling device varies from 0.1% to 9% of the stiffness  $k_1$  of the first story of the system. The viscous damping is initially neglected ( $c_C = 0$ ).

##### 4.3.1 Coupling device with no damping

The first case here discussed regards the coupling between the *2-DOF* representing a three stories frame structure and the block (first row of Table 1 and Table 2). The following geometrical parameters are taken fixed:  $d = 1m$ ,  $h_1 = 3m$  (see Fig. 2(a)). It can be demonstrated that the presented results are generally independent from the specific value of  $d$ , provided that the rotations of the block are small and that the stiffness  $k_C$  is itself independent from the length of the elastic device. Such an aspect, that equally applies for the external device, can be grasped from Eq.(6), were the potential energy is affected by the variation of length of the device rather than by its initial length.

Fig. 3(a) shows the main characteristics of the coupled system, whereas in Fig. 3(b), the gain maps of the parameters  $\alpha_1$  and  $\alpha_2$  are organized in such a way that each row refers to a different

circular frequency of the harmonic excitation. Inside the light grey regions, the gain parameters are less than unity. Hence, these regions, which are named gain regions, represent combinations of the parameters for which the coupling with the rigid block is beneficial for the structure. As it is possible to observe, the extent of such regions depends on the frequency of the excitation. Inside this regions, the efficiency of the coupling with the block, measured by the gain parameters, strongly depends on the frequency as well. In particular, the lowest values (*i.e.* the best performance of the protection device) occurs for  $\Omega = 15 \text{ rad/s}$ , where the gain can reach 25% ( $\alpha_2 = 0.75$ ). In other words, the coupled system exhibits a maximum drift smaller than the maximum drift of the uncoupled system of 25%. The comparison with the linearised formulation will help to enlighten these results.

Fig. 4 shows the time-histories of  $u_1$ ,  $u_2 - u_1$  (drift) and  $\vartheta$ , referring to point  $A$  labelled in the gain maps of  $\Omega = 15 \text{ rad/s}$  of Fig. 3. Specifically, Fig. 4(a) shows the comparison between the drift  $u_2 - u_1$  of the coupled (thick line) and uncoupled (thin line) systems. Since the point  $A$  is inside the gain region, the coupled system outperforms the uncoupled one (*i.e.* it has smaller displacements). Instead, Fig. 4(b) shows the displacement  $u_1$  (thin line) and the rotation  $\vartheta$  (thick line). After the first oscillations, the motions of the mass  $m_1$  and the block synchronize. Given the positive directions of the displacement  $u_1$  and the rotation  $\vartheta$ , which are shown in Fig. 2(a), the mass  $m_1$  and the block synchronize in counter phase. In this case, the block works as a tuned mass damper for the frame structure.

In order to understand the real work of the coupled system, the linearised frequencies of the mechanical system are analysed. They are obtained by solving the eigenproblem of Eq. (14). With reference to an harmonic excitation with circular frequency  $\Omega = 15 \text{ rad/s}$ , the eigenvalues and the eigenvectors of the system are obtained for systems having the characteristics labelled  $A$ ,  $B$  and  $D$  in Fig. 3(b). Fig. 5 shows the results of such an analysis. Specifically, at the top of the figure, the circular frequency and the first mode shape of the uncoupled system are shown. Below, along the three columns, each one referring to a different point  $A$ ,  $B$  and  $D$ , the circular frequency and the mode shape of the three modes of the coupled system are shown, as well. As can be observed in Fig. 3(b), point  $A$  refers to a good performance of the system, since it is located close to a relative minimum of both the gain maps. At this point, the frequency of the excitation  $\Omega = 15 \text{ rad/s}$  is quite close to the frequency of the first mode of the uncoupled system and to the frequency of the second vibration mode of the coupled system as well. It is worth observing that in the second coupled mode the displacement of the connection point of the frame and the block are in counter phase. Hence, in this case the harmonic excitation, being in quite resonance with the uncoupled system, maximize its displacements; at the same time the closeness between the harmonic frequency and the one of the second mode of the coupled system, encourage the working as tuned mass damper of the block, minimizing the displacements of the frame. When a change of the mechanical characteristics of system is made, moving from point  $A$  to  $B$  and  $C$ , the spectral characteristics of the coupled system change as well. For example, at point  $B$ , that is out the gain region of the maps, the first mode of the coupled system acquires a frequency very close to the one of the excitation. In this case, the excitation is in quite resonance condition with a coupled mode where the frame displacements and the block are in phase. In such a way, the coupling is not able to minimize the displacement of the frame. It is interesting to observe that in the second coupled mode the frame structure and the block are in counter phase yet. Moving to the point  $D$  the situation further worsen, since both in the first and the second coupled modes, the frame and the block oscillate in phase.

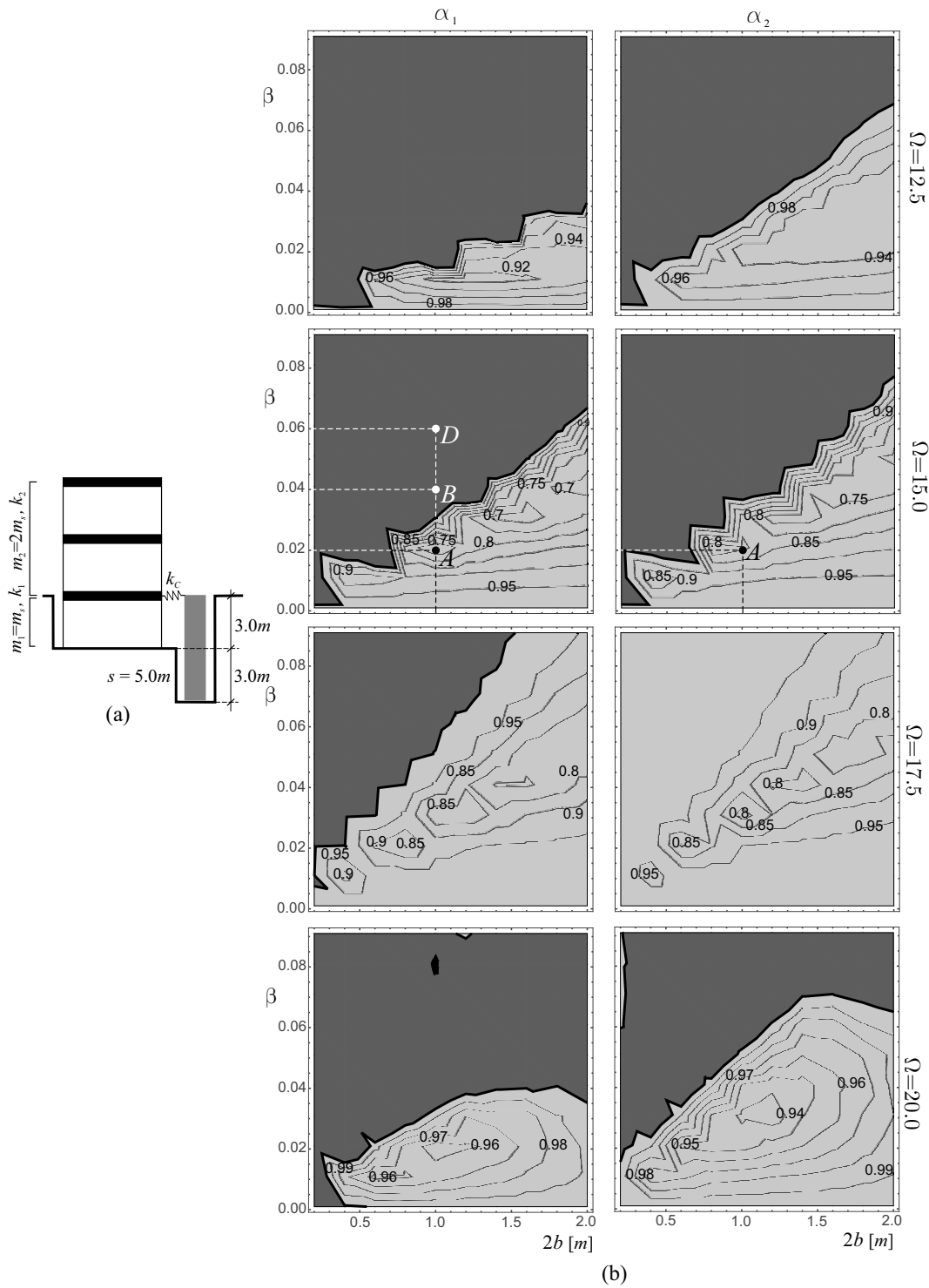


Fig. 3 Gain maps: (a) coupling scheme of the system representing a three stories frame and (b) gain maps for different circular frequencies of the harmonic excitation ( $A \equiv (2b = 1.0m; \beta = 0.02)$ ;  $B \equiv (2b = 1.0m; \beta = 0.04)$ ;  $D \equiv (2b = 1.0m; \beta = 0.06)$ )

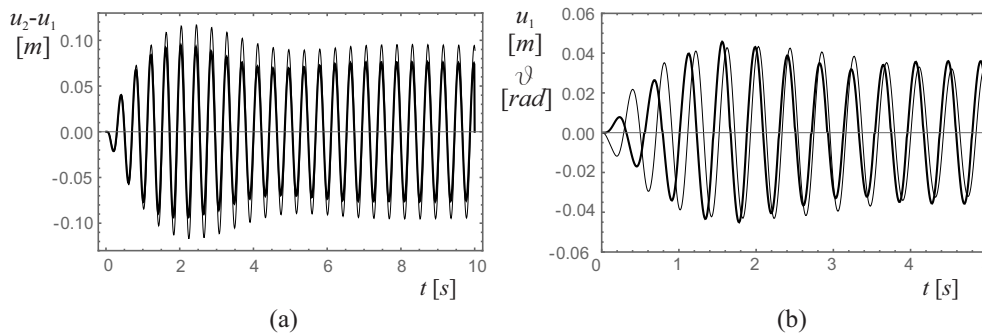


Fig. 4 Time-histories of the coupled system with characteristics labelled *A* in Fig. 3: (a) Drift  $u_2 - u_1$  of the coupled (thick line) and uncoupled (thin line) systems and (b)  $\vartheta$  (thick line) and  $u_1$  (thin line) of the coupled systems (same scale for  $\vartheta$  and  $u_1$ )

As further example, the same parametric analysis performed to obtain the gain maps of Fig. 3 is conducted for a 2-DOF, representing a five stories frame (second row of of Table 1 and Table 2). The following geometrical parameters are taken fixed:  $d = 1m, h_1 = 6m$  (see Fig. 2(a)). In Fig. 6(a) the main characteristics of the coupled system are shown, whereas in Fig. 6(b) several gain maps, referring to different frequencies of the harmonic excitation, are reported. As can be observed, gain regions exist also in this case. The extent of such regions depends on the frequency of the excitation, as well as the efficiency of the coupling, measured by the smallness of the gain parameters  $\alpha_1$  and  $\alpha_2$ , strongly depends on the harmonic frequency. The action of the coupling system can be explained in a similar way, already described in Fig. 5.

#### 4.3.2 Coupling device with damping

Finally the effects of the viscous damping of the coupling device is investigated. With reference to the system's characteristics labelled *A* in Fig. 3(b), whose resulting time-histories are shown in Fig. 4, the effects of an increasing viscous damping are analysed. The coefficient  $c_C$  (see Fig. 2(a)) is parametrized with respect to the damping coefficient of the frame  $c_1$ . In Fig. 7(a) the time evolution of the displacement  $u_1$  and of the angle  $\vartheta$  are shown in the same graphs, for different damping coefficients of the coupling device. As it can be observed, to an increase of the damping corresponds a decrease of the rocking amplitude of the block and, more important, a rephasing of the frame and the block motions. As a consequence, the operation as tuned mass damper of the block reduces by increasing the coupling damping. This fact is confirmed by the gain maps shown in Fig. 7(b). By comparing these maps with the ones in Fig. 3(b) (for  $\Omega = 15rad/s$ ), it is evident how the damping reduce both the extent of the gain regions and the efficiency of the coupling, since the values of  $\alpha_1$  and  $\alpha_2$  grow up in whole parameter plane with respect to the case without damping.

In order to better investigate the role of the coupling damping  $c_C$ , in Fig. 8 the  $\alpha_2$  gain maps, represented in the parameters plane  $\beta - c_C/c_1$ , are shown for different frequency  $\Omega$ . They are obtained by fixing the base of the block ( $b = 0.5m$ ) and varying both  $\beta$  and the ratio between  $c_C$  and  $c_1$ . As can be observed, for each frequency of the harmonic excitation, to an increase of the damping  $c_C$  (here parametrized with respect to  $c_1$ ) a reduction of the effectiveness of the coupling occurs. In fact, the best performances of the system, measured by the smallness of the gain coefficient  $\alpha_2$ , occur very close to the origin, where  $c_C = 0$ .

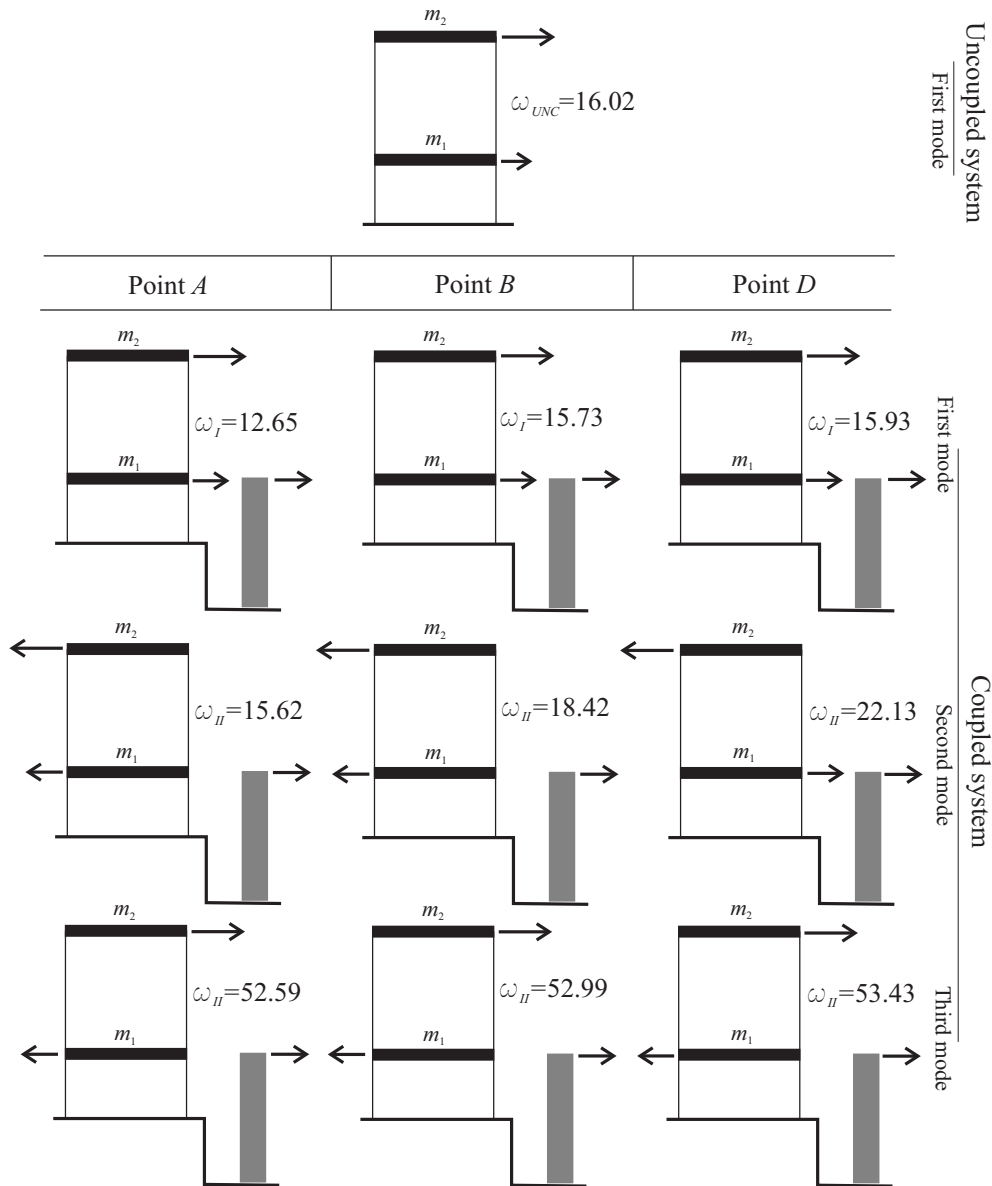


Fig. 5 Frequencies and mode shapes of the uncoupled and the coupled system (circular frequencies ( $rad/s^{-1}$ ))

#### 4.4 The role of both coupling and external visco-elastic devices

This Section investigates the effects on the motion of the frame structure of the external device of stiffness  $k_E$  and damping  $c_E$ , together with the coupling device (Fig. 2(a)).

The block base is always taken  $2b = 1.0m$ , corresponding to a block with mass  $M$  equal to about the 20% of the total mass of the system. The parameters that are varied in the analysis are the stiffness ratio  $\beta$  of the coupling device and the stiffness ratio  $\gamma$  of the external device (Eq. (15)). Both the stiffness varies in a range that goes from 0 to 20 times the stiffness of the first story  $k_1$ .

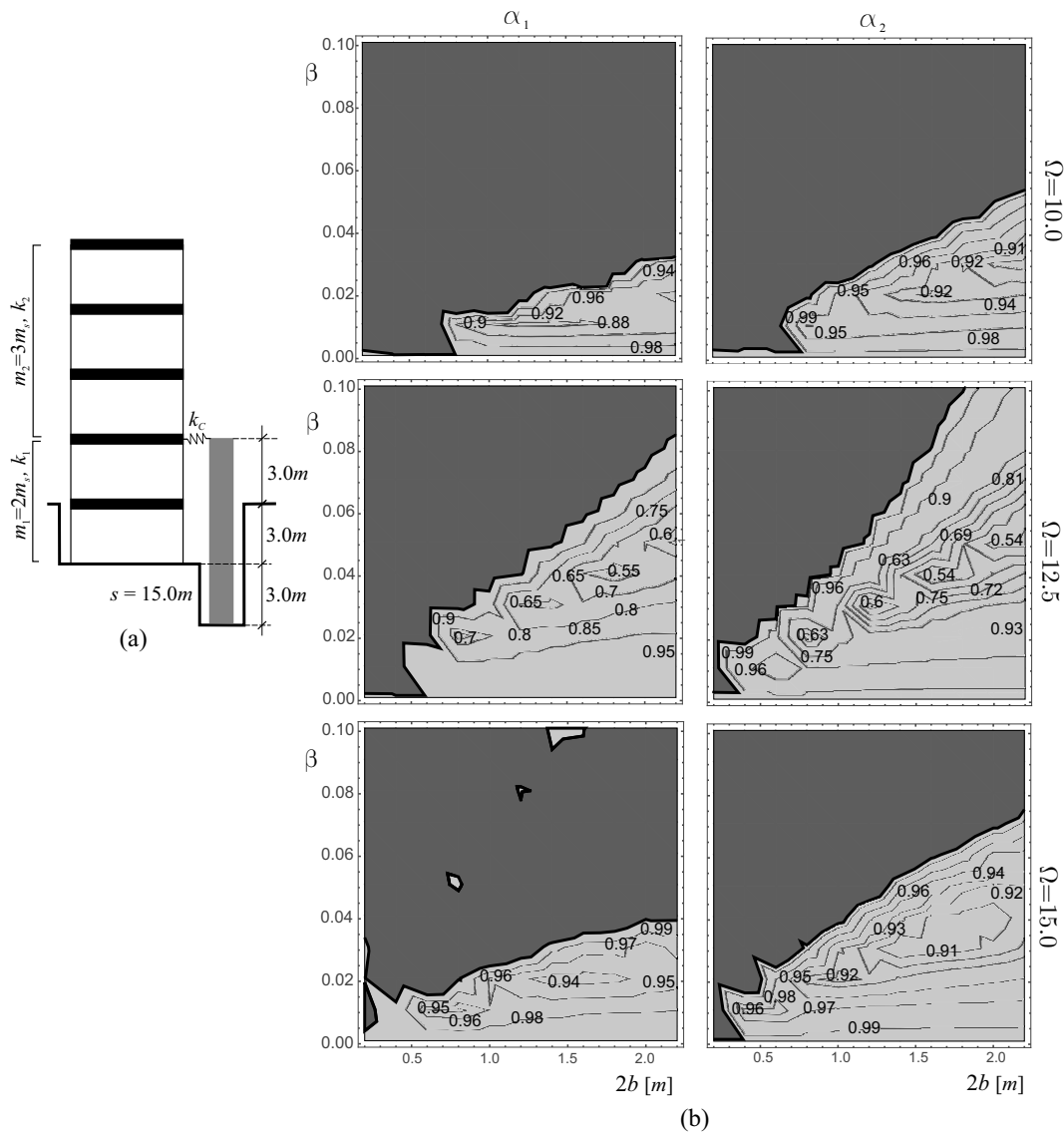


Fig. 6 Gain maps: (a) coupling scheme of the system representing a five stories frame and (b) gain maps for different circular frequencies of the harmonic excitation

It is worth observing that the effects of the external device can be achieved through different other types of devices. For example, the connection of the rocking block with the ground can be performed by using pre-stressed tendons as in Makris and Zhang (2001) or visco-elastic devices connecting the base corners of the block and the ground (Palmeri and Makris (2008)).

Initially, the viscous damping of such device is neglected ( $c_E = 0$ ).

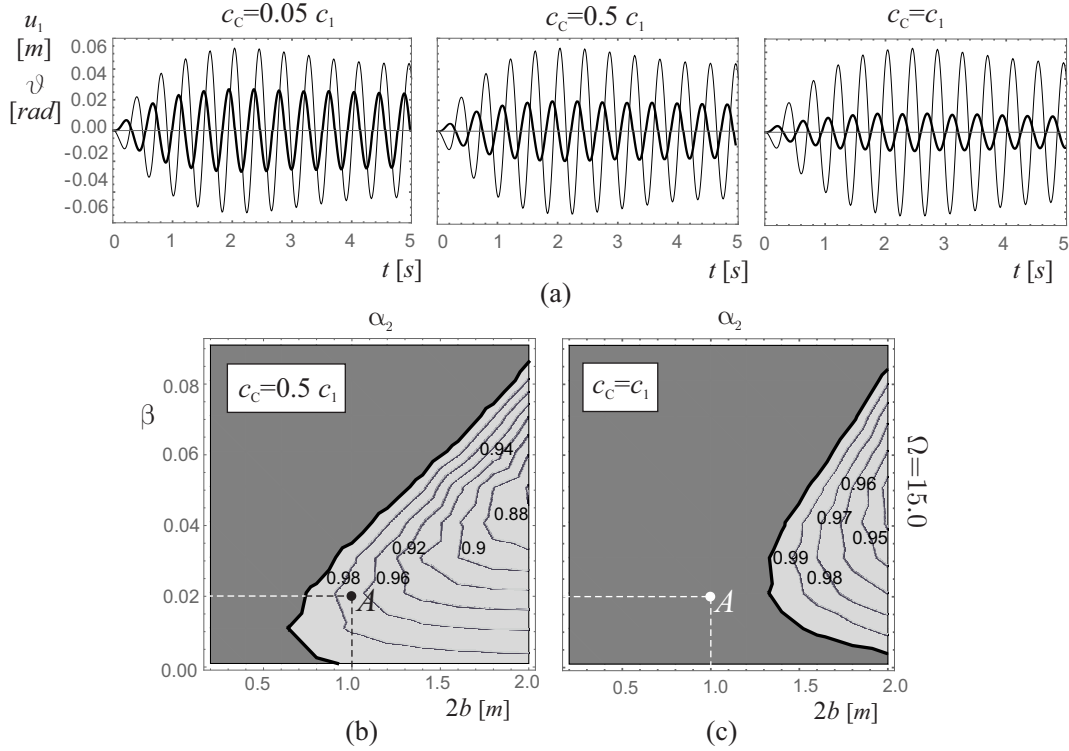


Fig. 7 Effects of the damping  $c_C$  of the coupling device: (a) Time-histories of the displacement  $u_1$  (thin line) and of the angle  $\theta$  (thick line) (same scale for  $\vartheta$  and  $u_1$ ) for different damping  $c_C$  (coupled system with characteristics labelled  $A$  in Fig. 3), (b) Gain maps obtained for  $c_C = 0.5c_1$  and (c) Gain maps obtained for  $c_C = c_1$

#### 4.4.1 External device with no damping

As a first instance, the coupling between the 2-DOF representing a three stories frame structure and the block (first row of Table 1 and Table 2) is evaluated with the following geometrical parameters being fixed:  $a = d = 1m, b = 0.5m, d_h = d_e, h_1 = 3m$  (see Fig. 2(a)) and hence no variability of the dimensions of the block is considered.

Fig. 9(a) shows the main characteristics of the coupled system, whereas in Fig. 9(b), the gain maps of the parameters  $\alpha_1$  and  $\alpha_2$  are organized as in Fig. 3. Inside the gain regions the combination of the coupling parameters is beneficial for the structure. The extent of such regions depends on the frequency of the excitation. Inside this regions, the efficiency of the coupling with the block, measured by the gain parameters, strongly depends on the frequency as well. In particular, the lowest values (*i.e.* the best performance of the protection device) occurs for  $\Omega = 15 rad/s$ . As can be observed, for each values of the excitation frequency  $\Omega$ , along the  $x$ -axis (*i.e.*, for  $\gamma = 0$ ) to very high values of  $\beta$  (high values of  $k_C$ ) always correspond no advantages for the coupled system. Hence, a perfectly rigid or a quite rigid connection between the frame and the block never corresponds to a dynamic improving of system behaviour.

In Fig. 10 the time-histories of  $u_1, u_2 - u_1$  (drift) and  $\vartheta$ , referring to point labelled  $E$  in the gain maps of  $\Omega = 15 rad/s$  of Fig. 9, are reported. Specifically, Fig. 10(a) shows the comparison between the drift  $u_2 - u_1$  of the coupled (thick line) and the uncoupled (thin line) systems. Also in

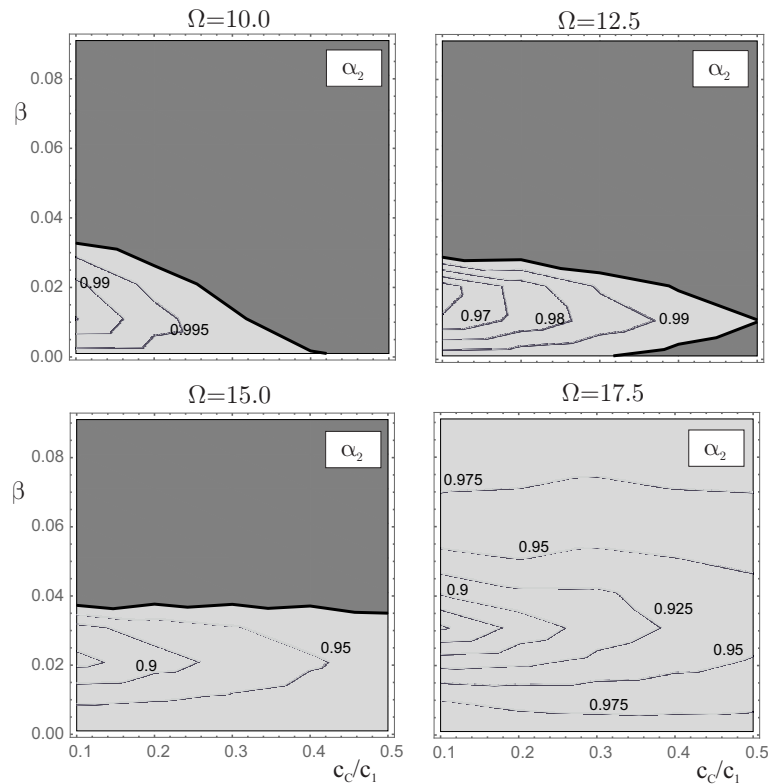


Fig. 8 Gain maps in the parameters plane  $\beta - c_C/c_1$ , for different frequencies of the harmonic excitation ( $b = 0.5m$ )

this case, the presence of the block improves the dynamics of the frame structure. Fig. 10(b) shows the corresponding displacement  $u_1$  (thin line) and rotation  $\vartheta$  (thick line). In this case, for the given positive directions of the displacements, the mass  $m_1$  and the block oscillate in phase. Hence, the main contribution to the improvement of the dynamics of the coupled system is provided by the external device.

The effectiveness of the coupling system is related mainly to two frequencies. Specifically, one is the frequency of the uncoupled system  $\omega_{unc}$  (see Table 2), the other is the frequency of the stand-alone super-structure of the coupled system  $\omega_2 = \sqrt{k_2/m_2}$  ( $\omega_2 = 19.75 \text{ rad/s}$ ). It is interesting to observe that along the diagonal of the gain maps of Fig. 9(b), the main frequency of the coupled system goes from the value  $\omega_{unc}$  (for  $\beta = \gamma = 0$ ) to the value  $\omega_2$  (for  $\beta \rightarrow \infty, \gamma \rightarrow \infty$ ).

Three different cases can occur: (i) if  $\Omega < \omega_{unc}$ , the frequency of the external excitation is closer to the uncoupled system one than to the frequency of the coupled system. In such a case, being the original system the more excited one, it results an advantage from the coupling with the block (see gain maps for  $\Omega = 12.5$  and  $\Omega = 15.0$  of Fig. 9(b)). Other case occurs when (ii)  $\omega_{unc} < \Omega < \omega_2$ . In this case, in the region of the parameters plane  $\beta - \gamma$  corresponding to frequencies of the coupled system close to the excitation one, no advantages occur since the coupled system is more excited than the uncoupled one. However, in the same parameter plane can exist gain regions sufficiently far from the previous one (see gain maps for  $\Omega = 17.5$  of Fig. 9(b)). The third case (iii) occurs when  $\Omega > \omega_2$ .

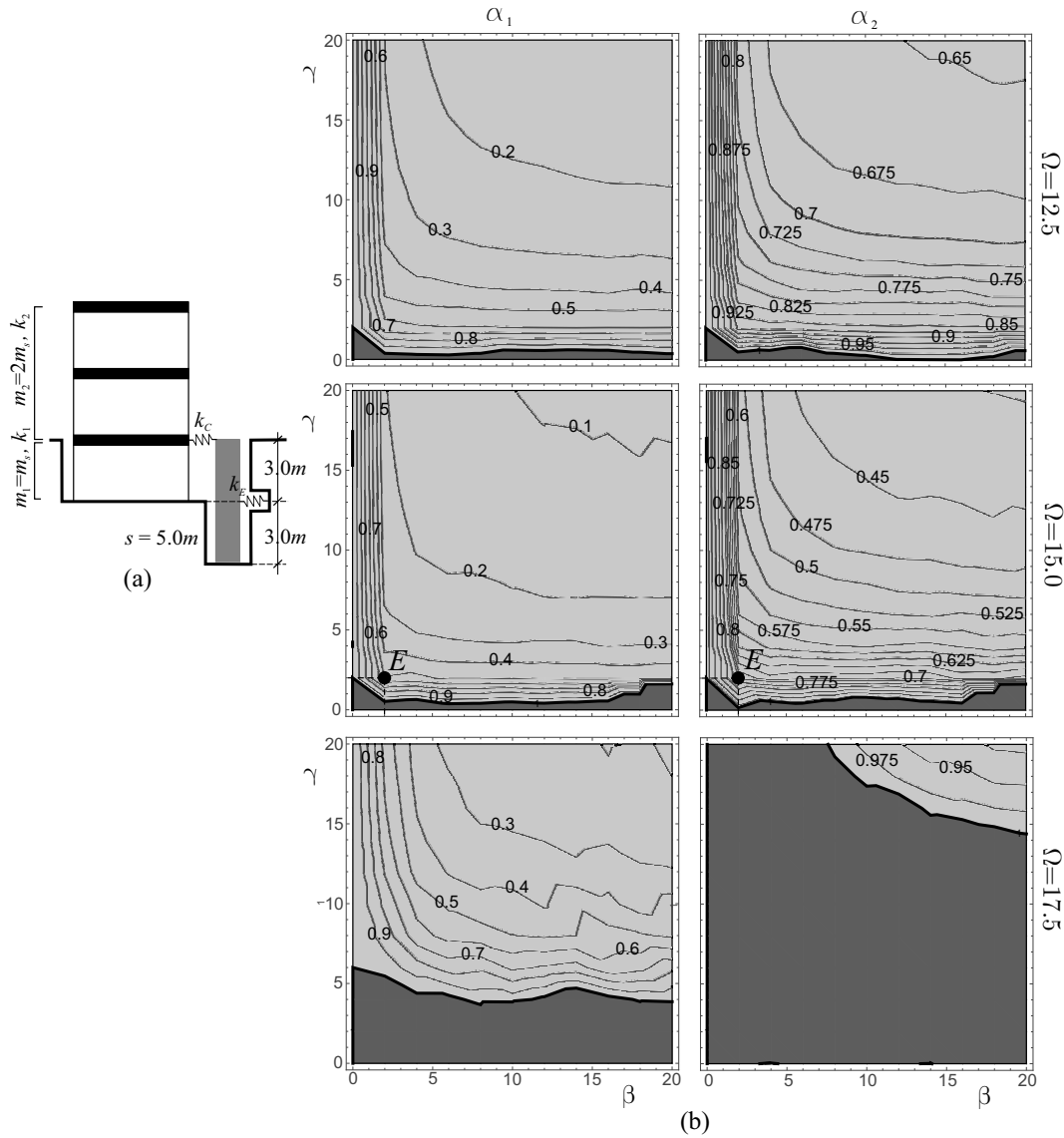


Fig. 9 Gain maps: (a) coupling scheme of the system representing a three stories frame and (b) gain maps for different circular frequencies of the harmonic excitation ( $E \equiv (\beta = 2; \gamma = 2)$ )

It can be demonstrated that in this last case the coupling is never effective.

As further example, a case regarding the coupling between the 2-DOF representing a five stories frame structure and the block (second row of Table 1 and Table 2) is discussed. The following geometrical parameters are taken fixed:  $a = d = 1m, b = 0.5m, d_h = d_e, h_1 = 6m$  (see Fig. 2(a)). Fig. 11(a) shows the main characteristics of the coupled system, whereas in Fig. 11(b), the gain maps of the parameters  $\alpha_1$  and  $\alpha_2$  are organized in such a way that each row refers to a different circular frequency of the harmonic excitation. Once again the maps show the direct influence of the frequency of the excitation upon the extent of the gain zones and on the efficiency of the coupling. The working

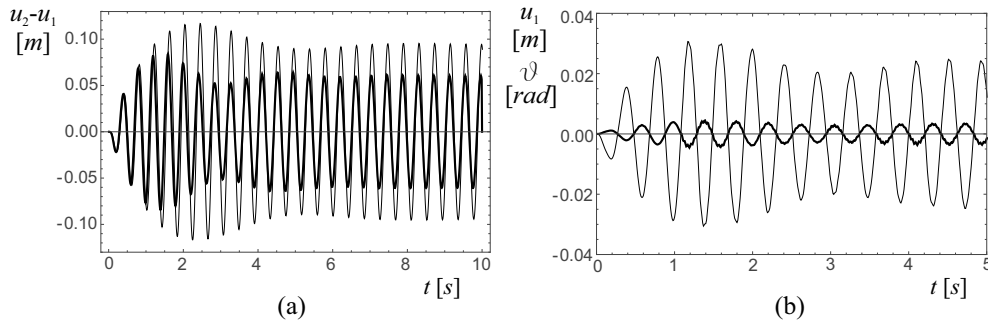


Fig. 10 Time-histories of the coupled system with characteristics labelled as  $E$  in Fig. 9: (a) Drift  $u_2 - u_1$  of the coupled (thick line) and uncoupled (thin line) systems and (b)  $\vartheta$  (thick line) and  $u_1$  (thin line) of the coupled systems (same scale for  $\vartheta$  and  $u_1$ )

of the coupled system can be interpreted as explained above for the 2-DOF model representing a three stories frame.

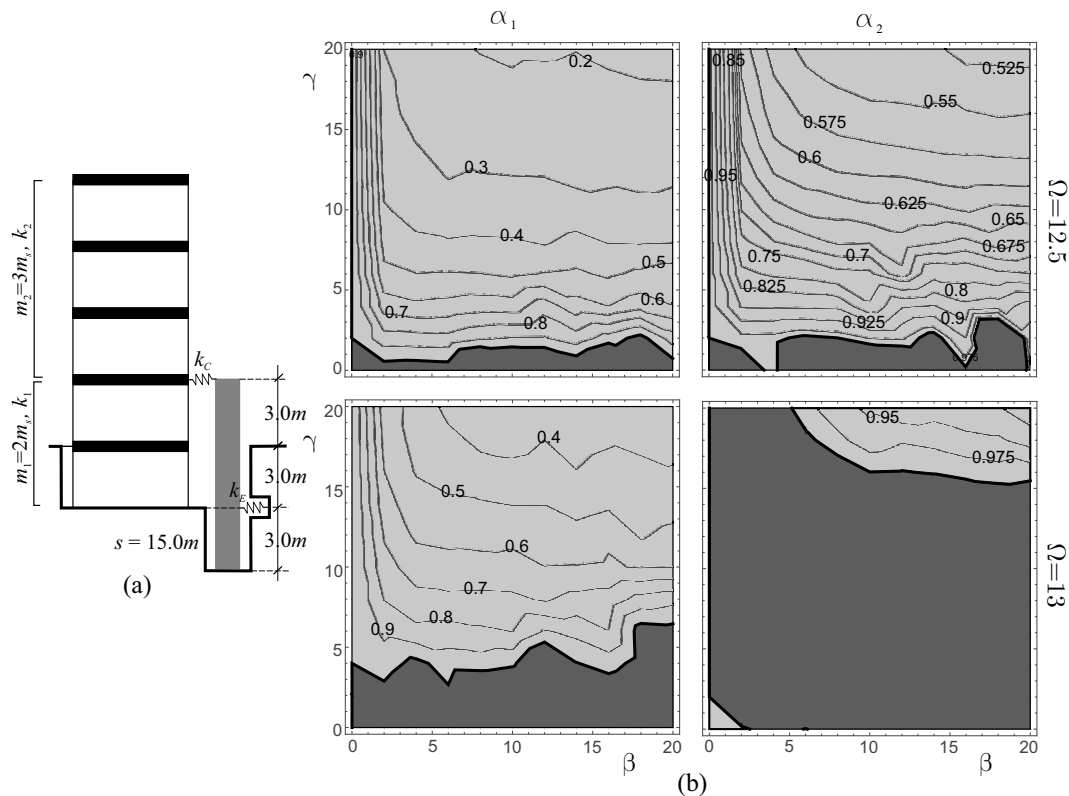


Fig. 11 Gain maps: (a) coupling scheme of the system representing a five stories frame and (b) gain maps for different circular frequencies of the harmonic excitation ( $\omega_2 = 14.18 \text{ rad/s}$ )

4.4.2 External device with damping

In this section the effects of the damping of the external device  $c_E$  is investigated. Since when both the coupling and the external devices are present, the frame and the block move in phase, it is expected that the coupling device works less than the external one. Hence, the attention will be focused only on the damping of the external device and it is taken  $c_C = 0$ .

In Fig. 12(a) two  $\alpha_2$  maps, referring to a 2-DOF that represents a three-stories frame are shown. They are both obtained for a circular frequency of the external excitation  $\Omega = 17 \text{ rad/s}$ , never used before. The two maps of Fig. 12(a) refer to two different value of damping coefficient  $c_E$  (parametrized with respect to the damping coefficient  $c_1$ ). From the two maps, it is possible to observe that the presence of damping makes the gain region more regular. Moreover, the no advantage region (dark grey region) becomes smaller than the case without damping. The length of the two segment  $\Delta\gamma_0$  and  $\Delta\gamma_1$ , in correspondence of a fixed  $\beta = 10$ , can be taken as measure of the extension of the dark grey region. The damping slight reduces this segment. In order to confirm this improving effect of the damping  $c_E$ , another parametric analysis is performed, whose results are shown in the maps of Fig. 12(b). It refers to the  $\alpha_2$  gain parameter, plotted in the parameter plane  $c_E/c_1 - \gamma$ , for fixed  $\beta$  ( $\beta = 10$ ). Along the vertical dashed lines, passing for  $c_E = 0$  and  $c_E = 5c_1$ , it is possible to read the segments  $\Delta\gamma_0$  and  $\Delta\gamma_1$  of the maps in Fig. 12(a). The decreasing of the vertical extent of the dark region, that occurs increasing the damping, shows that  $c_E$  has positive effects on the coupled system behaviour. The slight slope of the level curves of the map, also shows the small positive effects that the damping has on the gain parameter  $\alpha_2$ . In fact, by proceeding along an horizontal line ( $\gamma = \text{const.}$ ), a slight decreasing of the  $\alpha_2$  values occurs.

4.5 Final remarks

The summary of the previous results provides clear information about the range of the parameters and the working conditions for which the coupling with a rocking wall is beneficial for the system.

First, the case where only the coupling device is present, is considered. The following main aspects can be pointed out. Specifically:

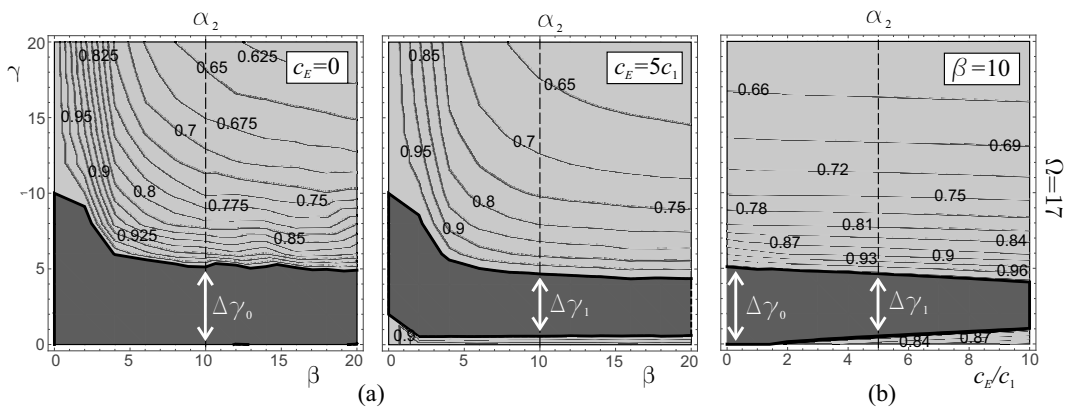


Fig. 12 Effects of the damping  $c_0$  of the external device: (a) Gain maps in the parameter plane  $\beta - \gamma$  for different damping  $c_E$  of the external device and (b) Gain maps in the parameter plane  $c_E/c_1 - \gamma$  for fixed stiffness  $k_C$  ( $\beta = 10$ ) of the coupling device ( $c_C = 0$ )

- The efficiency of the coupling proves to be higher for block with a sufficiently high base. For very small values of the base  $2b$ , the coupling is almost never beneficial for the system (see Fig. 3 and Fig. 6);
- A higher base  $2b$  requires a higher stiffness of the coupling device; however the stiffness ratio  $\beta$  that assures a good response of the coupled system is always sufficiently small ( $\beta < 0.09$ );
- From the previous analyses it can be asserted that the coupling works well when the frequency of the harmonic excitation is close to the one of the vibration mode where the wall and the first story moves in counter phase, thus assuring the working as tuned mass damper of the wall; since in general the frequency of such a mode is greater than the first frequency of the uncoupled system, the presence of the block assures the most beneficial effects for excitation frequencies higher than the first frequency of the uncoupled system.

Second, the case where both the coupling and the external devices are present, is considered. The following main aspects can be point out. Specifically:

- For all the considered base lengths  $2b$ , very high values of the stiffness ratios  $\beta$  and  $\gamma$  are necessary to assures good performances of the coupled system (see Fig. 9 and Fig. 11); in general both the stiffness  $k_C$  and  $k_E$  have to be higher than the stiffness of the first story of the system  $k_1$ ;
- From the previous analyses it can be asserted that the coupling works well when the frequency of the harmonic excitation is close or smaller than the first frequency of the uncoupled system; contrarily to the previous case, here the coupling assures the most beneficial effects for excitation frequencies smaller than the first frequency of the uncoupled system.

## 5. Conclusions

In the paper, a frame structure coupled with a rocking rigid block has been considered with the aim to improve the dynamics of the frame. The multi-story frame has been modelled as a two degree of freedom system that is connected to the block through a linear visco-elastic device. The model also includes a second visco-elastic device that connects the block to the ground. The non-linear equations of motion have been obtained by a Lagrangian approach and successively numerically integrated to analyse the behaviour of the coupled system. The coupling with the block has been considered beneficial for the frame structure when there is a reduction of the displacements of the structure. Simulations have been performed considering a harmonic excitation. The results of an extensive parametric analysis have been summarized in gain maps plotted in different planes of the system's parameters. The maps provide the ratio between the maximum displacement (or the drift) of the coupled system and the maximum displacement (or the drift) of the frame structure not coupled with the block. A ratio less than unity highlights the effectiveness of the block in improving the dynamics of the frame structure. Results have shown that the presence of the rocking rigid block improves the dynamics of the structure in two cases. In the first case, when only the internal coupling device is present, the block works as a tuned mass damper for the structure. This happens for very low values of the stiffness of the internal coupling device. In the second case, when both the devices are present, the block oscillates in phase with the bottom part of the structure. The resulting dynamics

is similar to the one that would be obtained increasing the mass and stiffness of the degree of freedom related to the bottom part of the frame structure, connected with the block.

In both cases, it is possible to improve the behaviour of the frame structure in wide ranges of the parameters' values.

## References

- Aghagholizadeh, M. and Makris, N. (2018), "Earthquake response analysis of yielding structures coupled with vertically restrained rocking walls", *Earthq. Eng. Struct. Dyn.*, **47**(15), 2965-2984. <https://doi.org/10.1002/eqe.3116>.
- Andreas, U. (1990), "Sliding-uplifting response of rigid blocks to base excitation", *Earthq. Eng. Struct. Dyn.*, **19**(8), 1181-1196. <https://doi.org/10.1002/eqe.4290190808>.
- Brzeski, P., Kapitaniak, T. and Perlikowski, P. (2016), "The use of tuned mass absorber to prevent overturning of the rigid block during earthquake", *Int. J. Struct. Stabil. Dyn.*, **6**(10), 1550075. <https://doi.org/10.1142/S0219455415500753>.
- Caliò, I. and Marletta, M. (2003), "Passive control of the seismic response of art objects", *Eng. Struct.*, **25**, 1009-1018. [https://doi.org/10.1016/S0141-0296\(03\)00045-2](https://doi.org/10.1016/S0141-0296(03)00045-2).
- Ceravolo, R., Pecorelli, M. and Zanotti Fragonara, L. (2016), "Semi-active control of the rocking motion of monolithic art objects", *J. Sound Vib.*, **374**, 1-16. <https://doi.org/10.1016/j.jsv.2016.03.038>.
- Ceravolo, R., Pecorelli, M. and Zanotti Fragonara, L. (2017), "Comparison of semi-active control strategies for rocking objects under pulse and harmonic excitations", *Mech. Syst. Signal Proc.*, **90**, 175-188. <https://doi.org/10.1016/j.ymsp.2016.12.006>.
- Collini, L., Garziera, R., Riabova, K., Munitsyna, M. and Tasora, A. (2016), "Oscillations control of rocking-block-type buildings by the addition of a tuned pendulum", *Shock Vib.*, **2016**, 8570538. <http://dx.doi.org/10.1155/2016/8570538>.
- Contento, A. and Di Egidio, A. (2009), "Investigations into benefits of base isolation for non-symmetric rigid blocks", *Earthq. Eng. Struct. Dyn.*, **38**(7), 849-866. <https://doi.org/10.1002/eqe.870>.
- Contento, A. and Di Egidio, A. (2014), "On the use of base isolation for the protection of rigid bodies placed on a multi-storey frame under seismic excitation", *Eng. Struct.*, **62-63**, 1-10. <https://doi.org/10.1016/j.engstruct.2014.01.019>.
- Corbi, O. (2006), "Laboratory investigation on sloshing water dampers coupled to rigid blocks with unilateral constraints", *Int. J. Mech. Solid.*, **1**(1), 29-40.
- de Leo, A., Simoneschi, G., Fabrizio, C. and Di Egidio, A. (2016), "On the use of a pendulum as mass damper to control the rocking motion of a non-symmetric rigid block", *Meccanica*, **51**(11), 2727-2740. <https://doi.org/10.1007/s11012-016-0448-5>.
- DeJong, M. and Dimitrakopoulos, E. (2014), "Dynamically equivalent rocking structures", *Earthq. Eng. Struct. Dyn.*, **43**(10), 1543-1563. <https://doi.org/10.1002/eqe.2410>.
- Di Egidio, A., Alaggio, R., Contento, A., Tursini, M. and Della Loggia, E. (2015), "Experimental characterization of the overturning of three-dimensional square based rigid block", *Int. J. Non-Lin. Mech.*, **69**, 137-145. <https://doi.org/10.1016/j.ijnonlinmec.2014.12.003>.
- Di Egidio, A. and Contento, A. (2009), "Base isolation of sliding-rocking non-symmetry rigid blocks subjected to impulsive and seismic excitations", *Eng. Struct.*, **31**, 2723-2734.
- Di Egidio, A. and Contento, A. (2010), "Seismic response of a non-symmetric rigid block on a constrained oscillating base", *Eng. Struct.*, **32**, 3028-3039. <https://doi.org/10.1016/j.engstruct.2010.05.022>.

- Di Egidio, A., de Leo, A. and Simoneschi, G. (2018), “Effectiveness of mass-damper dynamic absorber on rocking block under one-sine pulse ground motion”, *Int. Limit. Non-Lin. Mech.*, **98**, 154-162. <https://doi.org/10.1016/j.ijnonlinmec.2017.10.015>.
- Di Egidio, A., Simoneschi, G., Olivieri, C. and de Leo, A. (2014a), “Protection of slender rigid blocks from the overturning by using an active control system”, in “Proceedings of the 23rd Conference The Italian Association of Theoretical and Applied Mechanics”.
- Di Egidio, A., Zulli, D. and Contento, A. (2014b), “Comparison between the seismic response of 2D and 3D models of rigid blocks”, *Earthq. Eng. Eng. Vib.*, **13**(1), 151-162. <https://doi.org/10.1007/s11803-014-0219-z>.
- Dimitrakopoulos, E. and DeJong, M. (2012), “Overturning of retrofitted rocking structures under pulse-type excitations”, *J. Eng. Mech.*, **138**(8), 963-972. [https://doi.org/10.1061/\(ASCE\)EM.1943-7889.0000410](https://doi.org/10.1061/(ASCE)EM.1943-7889.0000410).
- Fabrizio, C., de Leo, A. and Di Egidio, A. (2017a), “Structural disconnection as a general technique to improve the dynamic and seismic response of structures: A basic model”, *Proc. Eng.*, **199**, 1635-1640. <https://doi.org/10.1016/j.proeng.2017.09.086>.
- Fabrizio, C., de Leo, A. and Di Egidio, A. (2019), “Tuned mass damper and base isolation: a unitary approach for the seismic protection of conventional frame structures”, *J. Eng. Mech.*, **145**(4), 04019011. [https://doi.org/10.1061/\(ASCE\)EM.1943-7889.0001581](https://doi.org/10.1061/(ASCE)EM.1943-7889.0001581).
- Fabrizio, C., Di Egidio, A. and de Leo, A. (2017b), “Top disconnection versus base disconnection in structures subjected to harmonic base excitation”, *Eng. Struct.*, **152**, 660-670. <https://doi.org/10.1016/j.engstruct.2017.09.041>.
- Housner, G. (1963), “The behavior of inverted pendulum structures during earthquakes”, *Bull. Seismol. Soc. America*, **53**(2), 404–417.
- Huang, W., McClurea, G. and Hussainzadab, N. (2013), “Seismic interactions between suspended ceilings and nonstructural partition walls”, *Coupled Syst. Mech.*, **2**(4), 329-348. <https://doi.org/10.12989/csm.2013.2.4.329>.
- Khawwaja, S., Nawawi and Chouw, N. (2013), “A shake table investigation on interaction between buildings in a row”, *Coupled Syst. Mech.*, **2**(2), 175-190. <https://doi.org/10.12989/csm.2013.2.2.175>.
- Kounadis, A.N. (2013), “Parametric study in rocking instability of a rigid block under harmonic ground pulse: a unified approach”, *Soil Dyn. Earthq. Eng.*, **45**, 125–143. <https://doi.org/10.1016/j.soildyn.2012.10.002>.
- Makris, N. and Aghagholizadeh, M. (2017), “The dynamics of an elastic structure coupled with a rocking wall”, *Earthq. Eng. Struct. Dyn.*, **46**(6), 945-954. <https://doi.org/10.1002/eqe.2838>.
- Makris, N. and Zhang, J. (2001), “Rocking response of anchored blocks under pulse-type motions”, *J. Eng. Mech.*, **127**(5), 484-493. [https://doi.org/10.1061/\(ASCE\)0733-9399\(2001\)127:5\(484\)](https://doi.org/10.1061/(ASCE)0733-9399(2001)127:5(484)).
- Muratović, A. and Ademović, N. (2015), “Influence of masonry infill on reinforced concrete frame structures’ seismic response”, *Coupled Syst. Mech.*, **4**(2), 173-189. <http://dx.doi.org/10.12989/csm.2015.4.2.173>.
- Ormeño, M., Tam Larkin, T. and Chouw, N. (2012), “Influence of uplift on liquid storage tanks during earthquakes”, *Coupled Syst. Mech.*, **1**(4), 311-324. <http://dx.doi.org/10.12989/csm.2012.1.4.311>.
- Palmeri, A. and Makris, N. (2008), “Response analysis of rigid structures rocking on viscoelastic foundation”, *Earthq. Eng. Struct. Dyn.*, **37**(7), 1039-1065. <https://doi.org/10.1002/eqe.800>.
- Pompei, A., Scalia, A. and Sumbatyan, M. (1998), “Dynamics of rigid block due to horizontal ground motion”, *J. Eng. Mech.*, **124**(7), 713-717. [https://doi.org/10.1061/\(ASCE\)0733-9399\(1998\)124:7\(713\)](https://doi.org/10.1061/(ASCE)0733-9399(1998)124:7(713)).
- Psycharis, I., M., F. and Stefanou, I. (2013), “Seismic reliability assessment of classical columns subjected to near-fault ground motions”, *Earthq. Eng. Struct. Dyn.*, **42**(14), 2061-2079. <https://doi.org/10.1002/eqe.2312>.
- Shenton, H. (1996), “Criteria for initiation of slide, rock, and slide-rock rigid-body modes”, *J. Eng. Mech.*,

- 122(7), 690-693. [https://doi.org/10.1061/\(ASCE\)0733-9399\(1996\)122:7\(690\)](https://doi.org/10.1061/(ASCE)0733-9399(1996)122:7(690)).
- Shenton, H. and Jones, N. (1991), "Base excitation of rigid bodies. I: Formulation", *J. Eng. Mech.*, **117**(10), 2286-2306.
- Simoneschi, G., de Leo, A. and Di Egidio, A. (2017a), "Effectiveness of oscillating mass damper system in the protection of rigid blocks under impulsive excitation", *Eng. Struct.*, **137**, 285-295. <https://doi.org/10.1016/j.engstruct.2017.01.069>.
- Simoneschi, G., Geniola, A., de Leo, A. and Di Egidio, A. (2017b), "On the seismic performances of rigid blocks coupled with an oscillating mass working as TMD", *Earthq. Eng. Struct. Dyn.*, **46**(9), 1453-1469. <https://doi.org/10.1002/eqe.2864>.
- Simoneschi, G., Olivieri, C., de Leo, A. and Di Egidio, A. (2018), "Pole placement method to control the rocking motion of rigid blocks", *Eng. Struct.*, **167**, 39-47. <https://doi.org/10.1016/j.engstruct.2018.04.016>.
- Spanos, P., Di Matteo, A., Pirrotta, A. and Di Paola, M. (2017), "Rocking of rigid block on nonlinear flexible foundation", *Int. J. Non-Lin. Mech.*, **94**, 362-374. <https://doi.org/10.1016/j.ijnonlinmec.2017.06.005>.
- Spanos, P. and Koh, A. (1984), "Rocking of rigid blocks due to harmonic shaking", *J. Eng. Mech.*, **110**(11), 1627-1642. [https://doi.org/10.1061/\(ASCE\)0733-9399\(1984\)110:11\(1627\)](https://doi.org/10.1061/(ASCE)0733-9399(1984)110:11(1627)).
- Spanos, P. and Koh, A. (1986), "Analysis of block random rocking", *Soil Dyn. Earthq. Eng.*, **5**(3), 178-183. [https://doi.org/10.1016/0267-7261\(86\)90021-7](https://doi.org/10.1016/0267-7261(86)90021-7).
- Taniguchi, T. (2002), "Non-linear response analyses of rectangular rigid bodies subjected to horizontal and vertical ground motion", *Earthq. Eng. Struct. Dyn.*, **31**(8), 1481-1500. <https://doi.org/10.1002/eqe.170>.
- Tung, C. (2007), "Initiation of motion of a free-standing body to base excitation", *Earthq. Eng. Struct. Dyn.*, **36**(10), 1431-1439. <https://doi.org/10.1002/eqe.703>.
- Vassiliou, M., K.R., M. and Stojadinović, B. (2014), "Dynamic response analysis of solitary flexible rocking bodies: modeling and behavior under pulse-like ground excitation", *Earthq. Eng. Struct. Dyn.*, **43**(10), 1463-1481. <https://doi.org/10.1002/eqe.2406>.
- Vassiliou, M. and Makris, N. (2012), "Analysis of the rocking response of rigid blocks standing free on a seismically isolated base", *Earthq. Eng. Struct. Dyn.*, **41**(2), 177-196. <https://doi.org/10.1002/eqe.1124>.
- VoyagakiIoannis, E., Psycharis, I. and Mylonakis, G. (2013), "Rocking response and overturning criteria for free standing rigid blocks to single-lobe pulses", *Soil Dyn. Earthq. Eng.*, **46**, 85-95. <https://doi.org/10.1016/j.soildyn.2012.11.010>.
- Yim, C., Chopra, A. and Penzien, J. (1980), "Rocking response of rigid blocks to earthquakes", *Earthq. Eng. Struct. Dyn.*, **8**(6), 565-587. <https://doi.org/10.1002/eqe.4290080606>.
- Zhang, J. and Makris, N. (2001), "Rocking response of free-standing blocks under cycloidal pulses", *J. Eng. Mech.*, **127**(5), 473-483. [https://doi.org/10.1061/\(ASCE\)0733-9399\(2001\)127:5\(473\)](https://doi.org/10.1061/(ASCE)0733-9399(2001)127:5(473)).
- Zulli, D., Contento, A. and Di Egidio, A. (2012), "Three-dimensional model of rigid block with a rectangular base subject to pulse-type excitation", *Int. J. Non-Lin. Mech.*, **47**(6), 679-687. <https://doi.org/10.1016/j.ijnonlinmec.2011.11.004>.

**A. Equations of motion for rocking of the block around the right corner**

Equations of motion for rocking of the block around the right corner read:

$$\begin{aligned}
 & k_C (2b \cos \theta - 2b - d + (d_h + h_1) \sin \theta + u_1) \times Q_3 + \\
 & c_C \left( \dot{\theta} ((d_h + h_1) \cos \theta - 2b \sin \theta) + \dot{u}_1 \right) + (c_1 + c_2) \dot{u}_1 - \\
 & c_2 \dot{u}_2 + (k_1 + k_2) u_1 - k_2 u_2 + m_1 (\ddot{x}_g + \ddot{u}_1) = 0 \\
 & \text{-----} \\
 & c_2 (\dot{u}_2 - \dot{u}_1) + k_2 (u_2 - u_1) + m_2 (\ddot{x}_g + \ddot{u}_2) = 0 \\
 & \text{-----} \\
 & d_e k_E (a \cos \theta + d_e \sin \theta) \times Q_4 + \\
 & k_C (\sin \theta (2b(2b + d) - 2bu_1 + d_h^2 + h_1 (2d_h + h_1))) \times Q_3 - \\
 & k_C ((d - u_1) (d_h + h_1) \cos \theta) \times Q_3 + \\
 & 4b^2 c_C \dot{\theta} + \ddot{\theta} J_B - 2bc_C \sin \theta \dot{u}_1 - bgM \cos \theta + bM \sin \theta \ddot{x}_g + c_E d_e^2 \dot{\theta} + \\
 & c_C d_h^2 \dot{\theta} + 2c_C d_h h_1 \dot{\theta} + c_C d_h \cos \theta \dot{u}_1 + c_C h_1^2 \dot{\theta} + c_C h_1 \cos \theta \dot{u}_1 - \\
 & gh_b M \sin \theta - h_b M \cos \theta \ddot{x}_g = 0
 \end{aligned} \tag{A.1}$$

where:

$$\begin{aligned}
 Q_3 &= \frac{\left( \sqrt{\frac{8b^2 - 2 \cos \theta (2b(2b + d) - 2bu_1 + d_h^2 + h_1 (2d_h + h_1)) + 4bd - 4bu_1 + -d}{d^2 - 2(d - u_1)(d_h + h_1) \sin \theta - 2du_1 + 2d_h^2 + 4d_h h_1 + 2h_1^2 + u_1^2}} \right)}{\sqrt{\frac{8b^2 - 2 \cos \theta (2b(2b + d) - 2bu_1 + d_h^2 + 2d_h h_1 + h_1^2) + 4bd - 4bu_1 +}{d^2 - 2(d - u_1)(d_h + h_1) \sin \theta - 2du_1 + 2d_h^2 + 4d_h h_1 + 2h_1^2 + u_1^2}}} \\
 Q_4 &= \frac{(\sqrt{a^2 + 2ad_e \sin \theta - 2d_e^2 \cos \theta + 2d_e^2} - a)}{\sqrt{a^2 + 2ad_e \sin \theta - 2d_e^2 \cos \theta + 2d_e^2}}
 \end{aligned} \tag{A.2}$$

Finally, the uplift condition around the right corner B reads:

$$\ddot{x}_g = -\frac{g}{\lambda} + \frac{[k_C u_1(t) + c_C \dot{u}_1(t)] (d_h + h_1)}{M h_b} \tag{A.3}$$